A new specimen of *Parabohaiornis martini* (Avialae: Enantiornithes) sheds light on early avian skull evolution

WANG Min[1,2]

(1 *Key Laboratory of Vertebrate Evolution and Human Origins of Chinese Academy of Sciences*, *Institute of Vertebrate Paleontology and Paleoanthropology*, *Chinese Academy of Sciences* Beijing 100044 wangmin@ivpp.ac.cn)
(2 *CAS Center for Excellence in Life and Paleoenvironment* Beijing 100044)

Abstract The Enantiornithes is the most speciose clade of Mesozoic avialans with over 60 named taxa reported from most continents that span the whole Cretaceous. Most of the fossil remains of this clade, as well as those of other early diverging avialans are preserved in two-dimensions. This complicates to extract detailed anatomical information from the skull, in which the composite elements are delicate and thus not easily observable through conventional methods. The scarcity of well-preserved early avialan skulls, as well as the limited number of specimens that have been analyzed using computed tomography scanning, consequently circumscribes a large morphological gap in the fossil record during the transition from the heavy and akinetic dinosaurian skull to the lightweight and kinetic bird skull. Here, we present a three-dimensional digital reconstruction of the skull and part of the cervical vertebrae of a new specimen of the enantiornithine *Parabohaiornis martini* from the Early Cretaceous of China. Our results demonstrate that *Parabohaiornis* retains the plesiomorphic non-avialan dinosaurian temporal and palatal reinforcing the recent hypothesis that the temporal and palatal regions are evolutionarily conservative and that the akinetic skull has been conserved well into of early branching avialans.

Key words Avialae, Bohaiornithidae, cranium, cranial kinesis, Enantiornithes

Citation Wang M, in press. A new specimen of *Parabohaiornis martini* (Avialae: Enantiornithes) sheds light on early avian skull evolution. Vertebrata PalAsiatica.

1 Introduction

The Bohaiornithidae is currently recognized as the most diverse enantiornithine family and that encompasses six known genera and species (*Bohaiornis guoi*, *Sulcavis geeorum*, *Zhouornis hani*, *Shenqiornis mengi*, *Parabohaiornis martini*, *Longusunguis kurochkini*) that persisted at least million years (125–120 Ma) (Wang et al., 2014a; Hu et al., 2020), which provides a rare chance to investigate taxonomical and morphological diversity during the early evolution of the Enantiornithes. Bohaiornithids also display several morphological features

国家自然科学基金杰出青年基金(批准号：42225201)、中国科学院前沿科学重点研究计划从“0到1”原始创新十年择优项目(编号：ZDBS-LY-DQC002)和腾讯科学探索奖支持。

收稿日期: 2023-01-04

that are readily distinguishable from other enantiornithines, such as the large subconical teeth with caudally curved tips, the lateral trabeculae of the sternum strongly directed caudolaterally that terminate with a fan-shaped expansion, and the presence of hyper-elongated pedal claws (Wang X et al., 2010; Hu et al., 2011; O'Connor et al., 2013; Wang et al., 2014a). The available materials of bohaiornithids, including some taxa represented by multiple specimens that preserve postcranial elements in views, has likely made their postcranial anatomy the best known among enantiornithines. Comparatively, our understanding of the cranial morphologies of bohaiornithids is still restricted to the facial and jaw bones, leaving the morphology of the temporal and palatal regions poorly investigated. This is unfortunate due to the fact that, the temporal and palatal structures are functionally critical to certain aspects of the avian skull, such as the cranial kinesis, which is a unique functional property that allows the upper jaw to move independently of the braincase and lower jaw. This feature is due to its contribution to the enormous radiation of the crown birds (Bock, 1964; Zusi, 1984; Lovette and Fitzpatrick, 2016). Here we describe a new bohaiornithid specimen which is referrable to *Parabohaiornis martini* on basis of preserving diagnostic characters of this taxon. The specimen is unearthed from the Early Cretaceous Jiufotang Formation at the Lamadong Town (119 Ma; Yu et al., 2021), Jianchang County, Liaoning Province, Northeastern China, where the holotype and referred specimens of *Parabohaiornis* were collected (Wang et al., 2014a). Considering that the postcranial morphologies of *Parabohaiornis* have been sufficiently covered in previous studies, the present work only focuses on the cranium. The excellently preserved skull in the new specimen, augmented through x-ray computed tomography (CT) scanning, compensates previously unrecognized cranial features with

2 Materials and methods

Computed tomography imaging In order to improve the resolution of CT scanning, the skull and the articulated cranial six cervical vertebrae of IVPP V28398 have been extracted from the slab. Then the block was scanned using the industrial CT scanner Phoenix v-tome-x at the Institute of Vertebrate Paleontology and Paleoanthropology, Chinese Academy of Sciences (IVPP) in Beijing, with beam energy of 160 kV and a of 130 μA at a resolution of 17.911 μm. The resulting scanned images were imported into Avizo (v. 9.2.0) for digital segmentation, rendering, and reconstruction.

Anatomical terminology primarily follows Baumel and Witmer (1993), using English equivalents for the Latin terms.

3 Systematic paleontology

Avialae Gauthier, 1986

Ornithothoraces Chiappe, 1995

Enantiornithes Walker, 1981

Bohaiornithidae Wang et al., 2014a

***Parabohaiornis martini* Wang et al., 2014a**

Revised diagnosis A medium-sized bohaiornithid enantiornithine that is distinguishable from other bohaiornithids in preserving the following combination of characters (asterisk marks autapomorphy): maxilla bearing four teeth; nasal perforated by a foramen*; concave dorsal margin of lacrimal*; surangular bearing a lateral fossa*; scapular with an acromion process oriented in parallel to the shaft in lateral view; tibiotarsus without an intercondylar incisure; length ratio of pygostyle to metatarsal III of 0.92–0.99; and a proximal phalanx of pedal digit IV proportionately shorter than in other bohaiornithids relative to the penultimate phalanx of digit IV (this ratio <70% in *Parabohaiornis*, but >80% in other bohaiornithids) Wang et al., 2014a)

Remarks IVPP V28398 is larger than the two known specimens of *Parabohaiornis*: specifically, the humerus is 21% and 12% longer than the holotype IVPP V18691 and the referred specimen V18690, respectively (Figs. 1,2; Table 1). The new specimen is also

Table 1 Selected measurements of IVPP V28398 in comparison with other *Parabohaiornis martini* (V18691: holotype; V18690: referred specimen; data from Wang et al., 2014a) (mm)

Specimen (length)	V18691	V18690	V28398
Skull	42.5		44.1
Coracoid	21.9	25.6	28.3*
Scapula	33.3		41.2
Humerus	43.4	46.7	52.5
Ulna	43.8		55.7
Radius	40.3		52.7*
Alular metacarpal	3,9		4.2
Alular digit 1	8.1		9.5
Alular digit 2	3.5		4.3
Major digit 1	10.2		10.9
Major digit 2	7.4		7.8
Major digit 3	3.2		3.5
Minor digit 1	5.5		5.8
Pygostyle	18.0	21.8	24.1*
Tibiotarsus	40.0	45.0	54.4
Metatarsal II	17.1	20.4	23.7
Metatarsal III	19.5	22.0	26.7
Metatarsal IV	18.1	20.6	24.3
Digit I-1	5.4	6.1	6.1
Digit I-2	6.0	6.3*	6.8
Digit II-1	4.5	5.8	6.2
Digit II-2	6.8	7.6	8.5
Digit III-1	6.4	7.8	7.6
Digit III-2	5.4	6.5	8.2
Digit IV-1	2.9	2.9	3.7
Digit IV-2	2.6	2.6	3.4
Digit IV-3	2.9	2.9	3.4
Digit IV-4	4.1	4.4	4.3

* estimated value.

Fig. 1 Photograph of the new referred specimen of *Parabohaiornis martini*, IVPP V28398
Abbreviations: ald. alular digit; am. alular metacarpal; ca. caudal vertebra; ce. cervical vertebra; co. coracoid; dv . hyoid; il. ilium; is. ischium; ma. major metacarpal; mad. major digit; mi. minor metacarpal; mid. minor digit; pu. pubis; py. pygostyle; p-I to p-IV. pedal digit I to IV; ra. radius; sc. scapula; sk. skull; st. sternum; sy. synsacrum; ti. tibiotarsus; tm. tarsometatarsus; un. ulna; /r(l). left (right) side. Scale bar = 20 mm

considered to be more osteologically more mature than those two specimens based on the complete fusion of all its compound elements, most notably the fusion of the tibiotarsus and tarsometatarsus which remain unfused in V18690 and V18691.

Fig. 2 Detailed postcranial features of the referred specimen of *Parabohaiornis martini*, IVPP V28398
A. pectoral region; B. distal hindlimb
Abbreviations: ci. capital incisure; m-I to m-IV. metatarsal I to IV; other abbreviations seen in Fig. 1
Anatomical features used to diagnose this specimen as *Parabohaiornis martini* are numbered:
1. omal ends of the scapula expanded; 2. acromion process of the scapula extending proximally in parallel to the shaft lateral view; 3. pygostyle without an abrupt distal constriction;
4. pedal digit II much robust than other pedal digits. Scale bars = 20 mm

4 Description

As in the holotype (Wang et al., 2014a), the premaxillary corpus (the region rostral to the frontal and maxillary process) is as dorsoventrally deep as it is rostrocaudally long. The frontal processes are partially medially fused with a suture only faintly discernable along their distal halves (Figs. 3, 4), a feature otherwise unknown amongst studied enantiornithines (O'Connor and Chiappe, 2011; Hu et al., 2020). This feature cannot be determined in the holotype due to the lack of exposure. The elongate frontal processes, despite not reaching the frontals, extend

Fig. 3 Photograph (A) and line drawing (B) of the cranial anatomy of the referred specimen of *Parabohaiornis martini*, IVPP V28398

Abbreviations: bp. basipterygoid process; bt, basal tubera; de. dentary; dpm. dorsal process of maxilla; fpp. frontal process of premaxilla; fr. frontal; hy. hyoid; jpm. jugal process of maxilla; ju. jugal; lc. lacrimal; mx. maxilla; na. nasal; oc. occipital condyle; pm. premaxilla; pr. parietal; qd. quadratojugal; qu. quadrate; sa. surangular-articular; sc. scleral ossicle; sp. splenial; /r(l). left (right) side. Scale bars = 10 mm

well beyond the rostral margin of the antorbital fenestra, and they are proportionately much longer than in some enantiornithines such as *Yuanchuavis* and *Eoenantiornis* (Zhou et al., 2005; Wang et al., 2022). CT scanning reveals four premaxillary teeth on each side (Fig. 4B), as is typical of enantiornithines including *Bohaiornis* (O'Connor and Chiappe, 2011; Wang et al., 2014a). Previous studies have estimated that there are three premaxillary teeth in the holotype on the basis of the exposed left premaxilla, which was further optimized to diagnose this taxon (Wang et al., 2014a). However, the caudal end of its maxillary process ends abruptly and therefore is likely incomplete in the holotype, and this prevents further observation whether or not an additional tooth exists in life. The rostral three premaxillary teeth are closely packed, with the fourth one separated from the rest by a noticeable gap. As in the holotype (Wang et al., 2014a), the first premaxillary tooth is smaller than the following ones. The triradiate maxillary bears four teeth with the caudalmost one level with the dorsal process, which concurs with the observation of the holotype (Wang et al., 2014a). The caudal end of the jugal process of the maxilla slants caudoventrally (Fig. 4B), resembling the condition observed in *Bohaiornis* and *Yuanchuavis* (Hu et al., 2011; Wang et al., 2022). This morphology remains elusive in the holotype of *Parabohaiornis* and other bohaiornithids due to poor preservation.

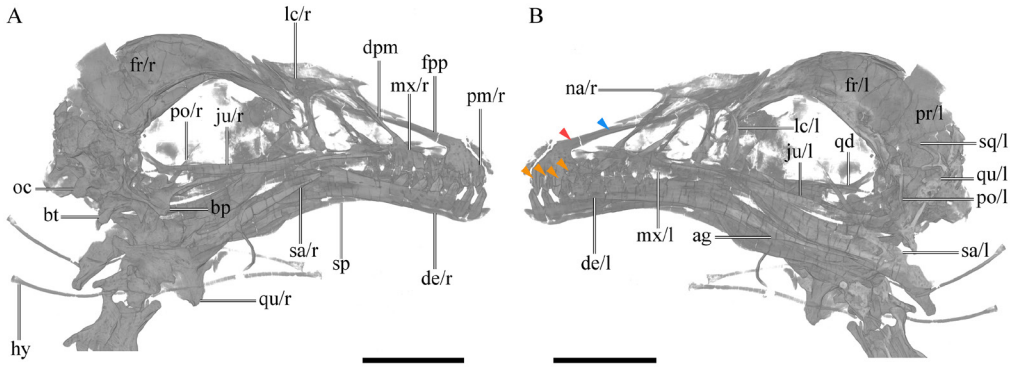

Fig. 4 Cranial anatomy of the referred specimen of *Parabohaiornis martini*, IVPP V28398
CT scanning of the skull in right lateral (A) and left lateral (B) views
The orange arrowheads denote the four premaxillary teeth on the left side. The red arrowhead indicates the fused proximal ends of the frontal processes of premaxilla that are separated distally (blue arrowhead)
Abbreviations: ag. angular; po. postorbital; sq. squamosal; other abbreviations seen in Fig. 3
Scale bars = 10 mm

A previous study claimed that the nasals of *Parabohaiornis* lacked the maxillary process as seen in *Shenqiornis* and *Bohaiornis* (Wang et al., 2014a). However, the preserved nasals exhibit uneven ventral margins, making it impossible to verify the original description. Our digital reconstruction of the right nasal of the new specimen reveals that the maxillary process is in fact present and is sharply tapered ventrally (Fig. 5A, B), resembling the condition seen in *Sulcavis*, *Zhouornis*, and *Longusunguis* (O'Connor et al., 2013; Zhang et al., 2013; Wang et al., 2014a). The whole element is generally vaulted laterally. The tapering rostral end of the nasal projects substantially more rostrally than the maxillary process, contrasting

with the subtle discrepancy observed in *Bohaiornis* (Hu et al., 2011). The dorsal margin of the nasal is weakly convex, rather than concave as in *Yuanchuavis* (Wang et al., 2022). This feature remains elusive in other bohaiornithids due to poor preservation. As in *Pengornis* but unlike other enantiornithines including other bohaiornithids (Zhou et al., 2008; O'Connor and Chiappe, 2011; O'Connor et al., 2013; Zhang et al., 2013; Wang et al., 2014a), the right nasal is perforated by a foramen (Fig. 5A). This foramen cannot be determined in the left nasal due to poor preservation. The smooth margin of that foramen in the right nasal suggests that it is genuine rather than a result of a preservational artefact. The corresponding areas of both nasals in the holotype are broken. Here the presence of that nasal foramen is considered to be a diagnostic character of *Parabohaiornis*.

The T-shaped lacrimal bears a rostral ramus that is stouter and shorter than the caudal ramus, and together they a central dorsal concavity (Fig. 5C, D), a feature which has so far only been found in *Pengornis* and *Piscivorenantiornis* among enantiornithines (Zhou et al., 2008; O'Connor and Chiappe, 2011). The robust ventral ramus inclines rostroventrally and is

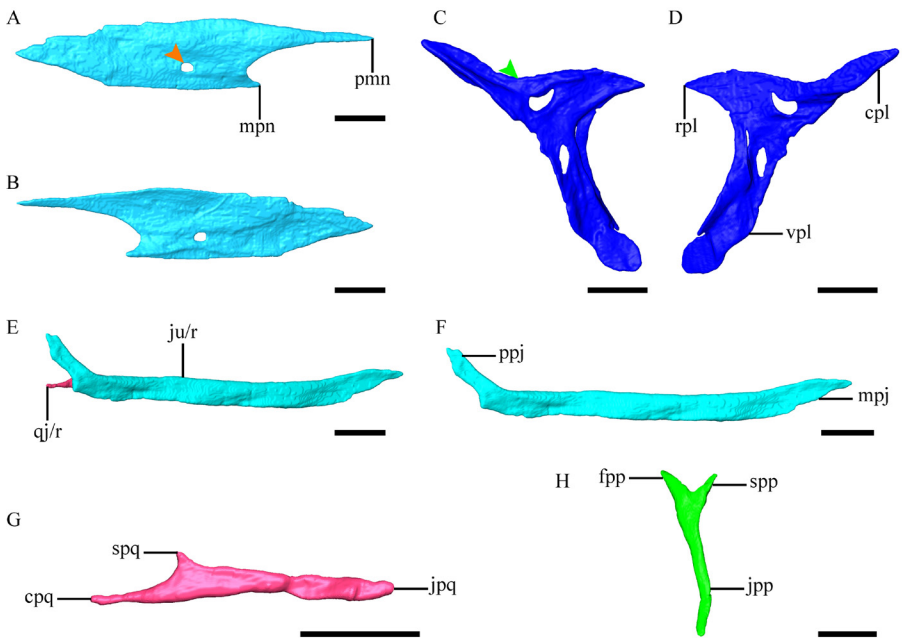

Fig. 5 Anatomy of selected cranial bones of *Parabohaiornis martini*, IVPP V28398

Digital reconstruction of the right nasal in lateral (A) and medial (B) views, right lacrimal in lateral (C) and medial (D) views, overlapping right jugal and quadratojugal in lateral view (E), right jugal in lateral view (F), right quadratojugal in medial view and mirrored (G), and left postorbital in lateral view (H)

The orange arrowhead in A denotes the foramen in the nasal, and the green arrowhead in C indicates the concave dorsal margin of the lacrimal

Abbreviations: cpl. caudal process of lacrimal; cpq. caudal process of quadratojugal; fpp. frontal process of postorbital; ju. jugal; jpp. jugal process of postorbital; jpq. jugal process of quadratojugal; mpj. maxillary process of jugal; mpn. maxillary process of nasal; pmn. premaxillary process of nasal; ppj. postorbital process of jugal; rpl. rostral process of lacrimal; spp. squamosal process of postorbital; spq. squamosal process of quadratojugal; vpl. ventral process of lacrimal; /r(l). left (right) side. Scale bars = 2 mm

longer than the dorsal rami. All these morphologies are identical to those of the holotype. CT scanning of the right lacrimal shows a crescent-shaped foramen in the juncture of the three rami and an oval-shaped foramen in the descending ramus. None of these two foramina can be in the holotype, despite the well-preserved right lacrimal of the specimen (Wang et al., 2014a). CT scanning of the left lacrimal of IVPP V28398 dose not reveal any sign of a ventral foramen (Fig. 4B), indicating that it is a preservational artefact. Unfortunately, the corresponding area in the juncture of the left lacrimal cannot be reconstructed with any real certainty, which prevents the determination of whether or not that foramen is genuine.

The jugal is relatively straight and tapers near the rostral extremity (Fig. 5E, F). Its caudal end, which is worn off in the holotype, is unforked and curves caudodorsally, as in *Bohaiornis* and *Yuanchuavis* (Hu et al., 2011; Wang et al., 2022), rather than forked as in some other enantiornithines such as *Shenqiornis*, *Longusunguis*, and *Falcatakely* (O'Connor and Chiappe, 2011; Wang et al., 2014a; O'Connor et al., 2020). There is a small element, overlain by the caudal end of the right jugal (Fig. 5E), that is interpreted as the quadratojugal, due to its proximity to the jugal and the fact that most of the cranial bones have been minimally displaced relative to each other. The quadratojugal measures approximately 1/3 the length of the jugal, and more than 4/5 of the quadratojugal has been overlain by the jugal. If this interpretation is correct, then the quadratojugal of *Parabohaiornis* is unique among enantiornithines in having a caudal process (Fig. 5G), which is a plesiomorphic feature widely distributed in non-avialan theropods but lost in most early avialans (Rauhut, 2003; Sullivan and Xu, 2017; Wang and Hu, 2017). The caudal process is slightly over half the length of the jugal process. Unlike the T-shaped morphology observed in most non-avialan theropods (Rauhut, 2003; Norell et al., 2006), the squamosal process is reduced to a short projection that measures approximately 1/10 of the length of the quadratojugal. A comparable reduction of the squamosal process has not been found in any other early diverging avialans including enantiornithines (Elżanowski and Wellnhofer, 1996; Rauhut, 2014; Wang and Hu, 2017; Wang et al., 2021), where the squamosal process is nearly as long as the jugal process (O'Connor and Chiappe, 2011; Wang et al., 2022; Li et al., 2023).

The postorbital, which is not preserved in the holotype, is preserved in its entirety on both sides (Fig. 4). This element has been identi in two bohaiornithids, *Shenqiornis* and *Longusunguis* (O'Connor and Chiappe, 2011; Hu et al., 2020). The T-shaped bone is more morphologically similar to that of *Longusunguis* in being delicate and having an elongate ventral ramus that is twice longer than the dorsal rami (Fig. 5H), from the large and broad form seen in *Shenqiornis* (O'Connor and Chiappe, 2011). The dorsal rami define an acute angle dorsally, contrasting with the weakly concave dorsal margin seen in *Shenqiornis*, *Longusunguis*, and *Yuanchuavis* (O'Connor and Chiappe, 2011; Hu et al., 2020; Wang et al., 2022). In the new specimen, the squamosal, an enigmatic cranial bone that has only been described in several early diverging avialans (O'Connor and Chiappe, 2011; Hu et al., 2020; Wang et al., 2022), remains articulated with the left quadrate (Fig. 6A). The bone is comparable

to that of *Longusunguis* in having an elongate pointed postorbital, quadratojugal processes, and a blunt paroccipital process (Fig. 6B–E) (Hu et al., 2020). The parietal process appears to be hidden by the paroccipital process in lateral view, which is likely in part due to compression. Unlike *Yuanchuavis*, *Archaeopteryx*, and some non-avialan theropods such as *Deinonychus* (Ostrom, 1969; Elżanowski and Wellnhofer, 1996; Wang et al., 2022), but as in enantiornithine IVPP V12707 and *Longusunguis* (Hu et al., 2020; Wang et al., 2021), the postorbital process is unforked rostrally. The rostroventrally oriented quadratojugal process is rod-like, in contrast with the rectangular form seen in *Yuanchuavis* (Wang et al., 2022). The caudal surface of the quadratojugal process is grooved along its entire length, giving it a V-shaped cross section (Fig. 6B, D), as in V12707 (Wang et al., 2021). The quadrate cotyla appears to be deeply inserted into the main body of the squamosal, and it is rostrocaudally longer than it is mediolaterally wide. However, this condition may have been exaggerated by compression. The parietal and paroccipital processes are much shorter than those observed in *Longusunguis* and V12707.

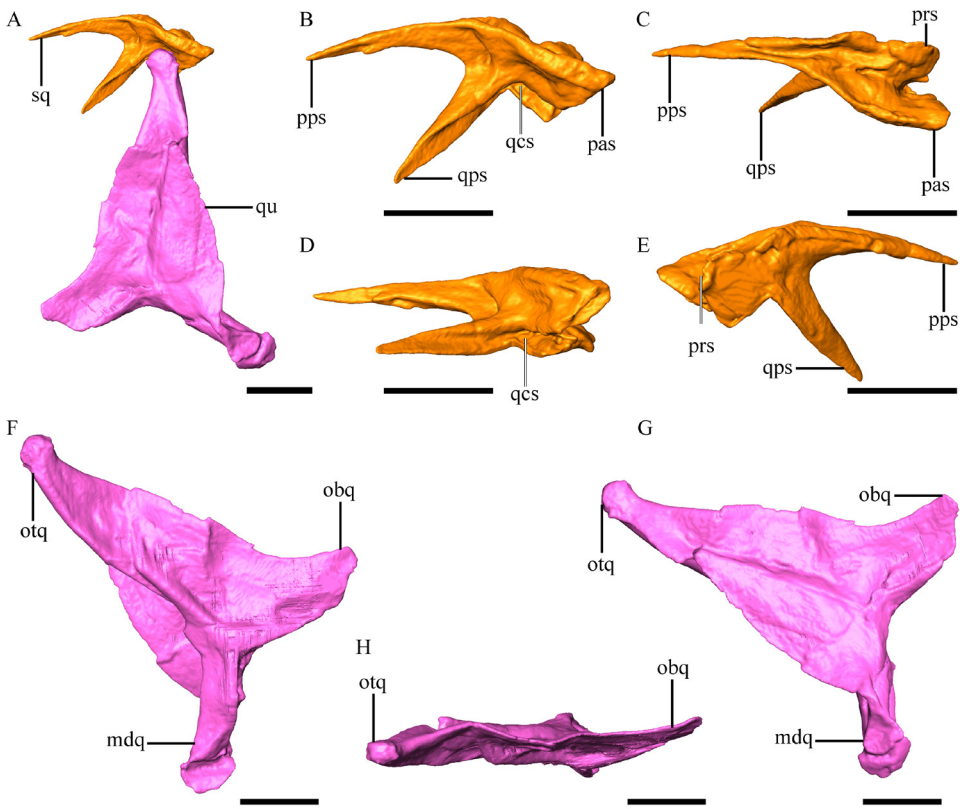

Fig. 6 Anatomy of temporal bones of *Parabohaiornis martini*, IVPP V28398
Digital reconstruction of the articulated left squamosal and quadrate (A), left squamosal in lateral (B), dorsal (C), ventral (D), medial (E) views, and left quadrate in rostrolateral (F), caudomedial (G), dorsal (H) views
Abbreviations: mdq. mandible process of quadrate; obq. orbital process of quadrate; otq. otic process of quadrate; pas. paraoccipital process of squamosal; pps. postorbital process of squamosal; prs. parietal process of squamosal; qcs. quadrate cotyla of squamosal; qps. quadratojugal process of squamosal; qu. quadrate; sq. squamosal. Scale bars = 2 mm

Both quadrates are severally compressed, particularly the mandibular process. Therefore, it is unclear whether or not a bicondylar condition is present as is the case in some other enantiornithines, e.g., *Shenqiornis* and *Longipteryx* (O'Connor and Chiappe, 2011; Stidham and O'Connor, 2021). The better-preserved dorsal portion of the quadrate is largely comparable to that of *Yuanchuavis* and non-avialan theropods. For instance, the orbital process is deep dorsoventrally and broadly convex rostrally, with a straight dorsal margin that extends to the otic process (Fig. 6F–G) (Hendrickx et al., 2015; Wang et al., 2022). In contrast, the orbital process is dorsoventrally much narrower in some enantiornithines such as *Longusunguis* and V12707 (Hu et al., 2020; Wang et al., 2021), and it is further into a sharply pointed shape in more crownward taxa such as *Hesperornis* (Lucas, 1903; Baumel and Witmer, 1993; Livezey and Zusi, 2006; Elżanowski and Stidham, 2011), which results in a deeply concave dorsal margin between the otic and orbital processes. However, the preserved shape of the orbital process in *Longusunguis* and V12707 can be attributed to ontogeny, given that the known specimens are skeletally immature. As in other enantiornithines (Stidham and O'Connor, 2021; Wang et al., 2022), the otic process is not divided into a squamosal and otic capitulum. In contrast to the condition seen in *Shenqiornis* and *Pengornis*, the caudal surface of the quadrate is not perforated by a foramen.

The frontals and parietals are severally crushed, providing few anatomical features other than those recognized in the holotype.

A mandibular symphysis is absent as in most other enantiornithines and early avialans (Fig. 4) (O'Connor and Chiappe, 2011). Same as in the typical condition of enantiornithines, the dentary has paralleling dorsal and ventral margins and a caudoventrally sloping caudal end. Six dentary teeth are present on each side. All these morphologies are identical to those of the holotype (Wang et al., 2014a). The post-dentary mandibular elements are well-preserved in the new specimen, whereas they are missing in the holotype. The articular and surangular are completely fused with one another, but they are not fused with the angular (Figs. 4, 7A, B). The surangular is sigmoid in lateral view, with its rostral two thirds bowed ventrally. The caudal third portion is dorsoventrally deeper than the rostral part and bears a lateral fossa close to the dorsal margin (Fig. 7B). A similar fossa is absent in most other enantiornithines, including *Bohaiornis*, *Longusunguis*, and *Gretcheniao* (Hu et al., 2011; Wang et al., 2014a; Chiappe et al., 2019). However, in *Fortunguavis* and some juvenile enantiornithines (e.g., IVPP V12707), the surangular is perforated by an oval foramen near the similar position (Chiappe et al., 2007; O'Connor and Chiappe, 2011; Wang et al., 2014b, 2021). Given that both specimens of IVPP V28398 and *Fortunguavis* holotype from osteologically mature individuals, the presence of this foramen/fossa cannot be unequivocally attributed to ontogeny as claimed in previous studies (Chiappe et al., 2007; O'Connor and Chiappe, 2011). Here we suggest that the fossa/foramen seen in those enantiornithines is homologous to the surangular foramen of non-avialan dinosaurs when considering their comparable anatomical positions (Weishampel et al., 2004; Norell et al., 2006). As in *Fortunguavis*, the medial process of the

mandible is robust and tapers as it projects mediocaudally. This structure cannot be recognized in other bohaiornithids due to poor preservation (*Sulcavis* and *Shenqiornis*) and/or lack of exposure (*Zhouornis*, *Longusunguis*, and *Bohaiornis*). The medial process is concave dorsally and separated from the quadrate cotyla by a rostromedially oriented crest. The quadrate cotyla is distinct with its long axis directed rostromedially (Fig. 7A). The rostral

half of the angular is spathulate in lateral aspect, and its caudal part is rod-like.

The cranial base of IVPP V28398 is relatively well-preserved. The basioccipital, basisphenoid, and parasphenoid appear to be fused with each other (Fig. 7B, C). As in *Zhouornis*, the occipital condyle is mediolateral wider than dorsoventrally high. The paired basal tubera is robust, projects ventrolaterally, and exceeds the occipital condyle in ventral projection, which is similae to the condition observed in some non-avialan theropods such as *Dromaeosaurus* and *Velociraptor* (Currie, 1995; Witmer, 1997; Barsbold and Osmólska, 1999). In contrast, this structure is reduced to a small swelling in *Archaeopteryx* (Rauhut, 2014; also in *Zhouornis*, see g. 2 in Zhang et al., 2013), some non-avialan theropods (e.g., *Saurornithoides*; Barsbold, 1974), *Hesperornis* (Elżanowski, 1991), and more crownward taxa with some exceptions such as penguins and long skulled birds (Baumel and Witmer, 1993; Bertelli et al., 2006). As in some theropods including early avialans such as *Archaeopteryx*, *Cratonavis*, *Zhouornis*, and IVPP V12707 (Zhang et al., 2013; Rauhut, 2014; Wang et al., 2021; Li et al., 2023), a large basisphenoid recess is developed, and it is rimed caudally by a crest that connects to the basal tubera (Fig. 7B). As in *Zhouornis*, V12707, and *Archaeopteryx*

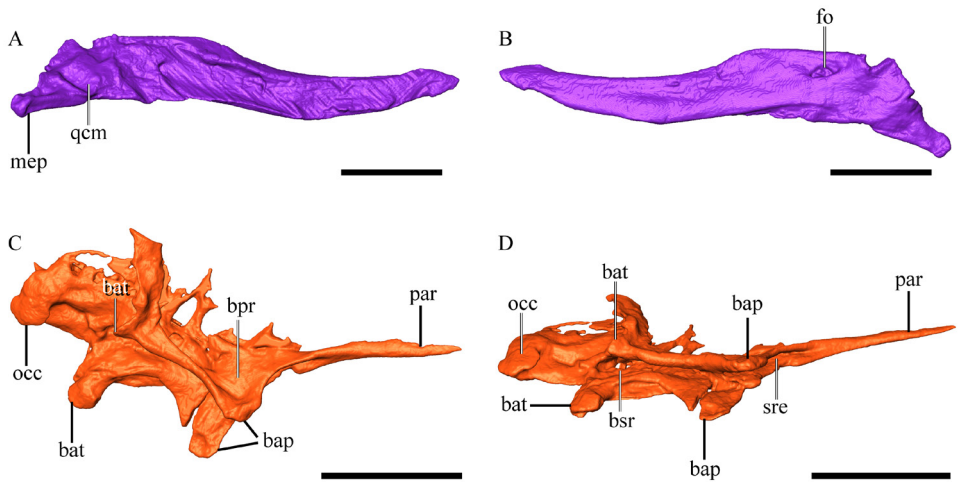

Fig. 7 Anatomy of selected elements of lower jaw and cranial base *Parabohaiornis martini*, IVPP V28398
Digital reconstruction of the left surangular-articular in medial (A) and lateral (B) views, basioccipital-basisphenoid-parasphenoid in lateral (C) and ventral (D) views
Abbreviations: bap. basipterygoid process; bat. basal tubera; bpr. basipterygoid recess; bsr. basisphenoid recess; fo. lateral fossa of surangular; mep. medial process of mandible; occ. occipital condyle; par. parasphenoid rostrum; qcm. quadrate cotyle of mandible; sre. subsellar recess. Scale bars = 5 mm

(Zhang et al., 2013; Rauhut, 2014; Wang et al., 2021), the basipterygoid processes are prominent. In contrast, this structure is greatly reduced in crownward taxa such as *Hesperornis* and most neognaths (Gingerich, 1976; Baumel and Witmer, 1993), but it is prominent in paleognaths (Livezey and Zusi, 2006; Wang et al., 2021). The basipterygoid processes appear to project as far ventrally as the basal tubera. In common with *Archaeopteryx* (Rauhut, 2014), the basipterygoid process bears a dorsal depression (Fig. 7C), which corresponds to the basipterygoid recess seen in non-avialan theropods (Currie, 1995; Witmer, 1997). However, that recess is absent in V12707 (Wang et al., 2021), and it remains unknown in *Zhouornis*. A deep subsellar recess is developed at the base of the parasphenoid rostrum (Fig. 7D), as in V12707 and some-nonavialan theropods such as *Velociraptor* (Bock, 1964; Barsbold and Osmólska, 1999; Wang et al., 2021). In contrast, that recess is absent in crown birds (McDowell, 1948). As in *Cratonavis* and the crown taxa (Livezey and Zusi, 2007; Li et al., 2023), the ventral surface of the parasphenoid rostrum is convex, lacking the trough present in V12707 and some non-avialan theropods (Currie and Zhao, 1993; Wang et al., 2021).

The cranial six cervicals, including the atlas and axis, loosely remain in articulation and are exposed dorsally (Figs. 1, 8). We digitally reconstructed the third and sixth cervicals and provide additional anatomical features that are not mentioned in the previous studies of the holotype and the referred specimen of *Parabohaiornis* (previous attempts to reconstruct the atlas and axis have been unsuccessful). As in other enantiornithines, the third to sixth cervicals are as craniocaudally long as mediolaterally wide (Fig. 8A, B), and lack the marked elongation seen in the contemporaneous ornithuromorphs, e.g., *Yanornis*, *Yixianornis*. The diverging pre- and postzygapophyses form an X-shaped contour in dorsal view, and the latter splay more laterally than the former (Fig. 8C). The neural spines are dorsoventrally low and fail to reach either the cranial nor the caudal margins of the associated centrum, as is the condition in other bohaiornithids (Zhang et al., 2013; Wang et al., 2014a). The ventral surface of the centrum is strongly keeled (Fig. 8B), which is also seen in *Sulcavis* and *Bohaiornis* but unknown in other bohaiornithids (Hu et al., 2011; O'Connor et al., 2013). Although compressed, the cranial and caudal articular facets of the cervical centra appear to be heterocoelous (Fig. 8E, F). The carotid processes, present in *Sulcavis* (O'Connor et al., 2013), are lacking. The cervical ribs are unfused with the third and fourth cervicals, but they are fused with the following two cervicals (Fig. 8B, D, H). In contrast, those ribs are all fused with the corresponding vertebrae in other bohaiornithids, e.g., *Zhouornis*, *Bohaiornis*. It should be noticed that the ribs are unfused with the last two cervicals but are fused with the preceding four vertebrae in the holotype of *Sulcavis* (O'Connor et al., 2013). However, due to poor preservation, the identitification of these cervicals cannot be properly determined in that particular specimen, thus preventing any direct comparison with IVPP V28398.

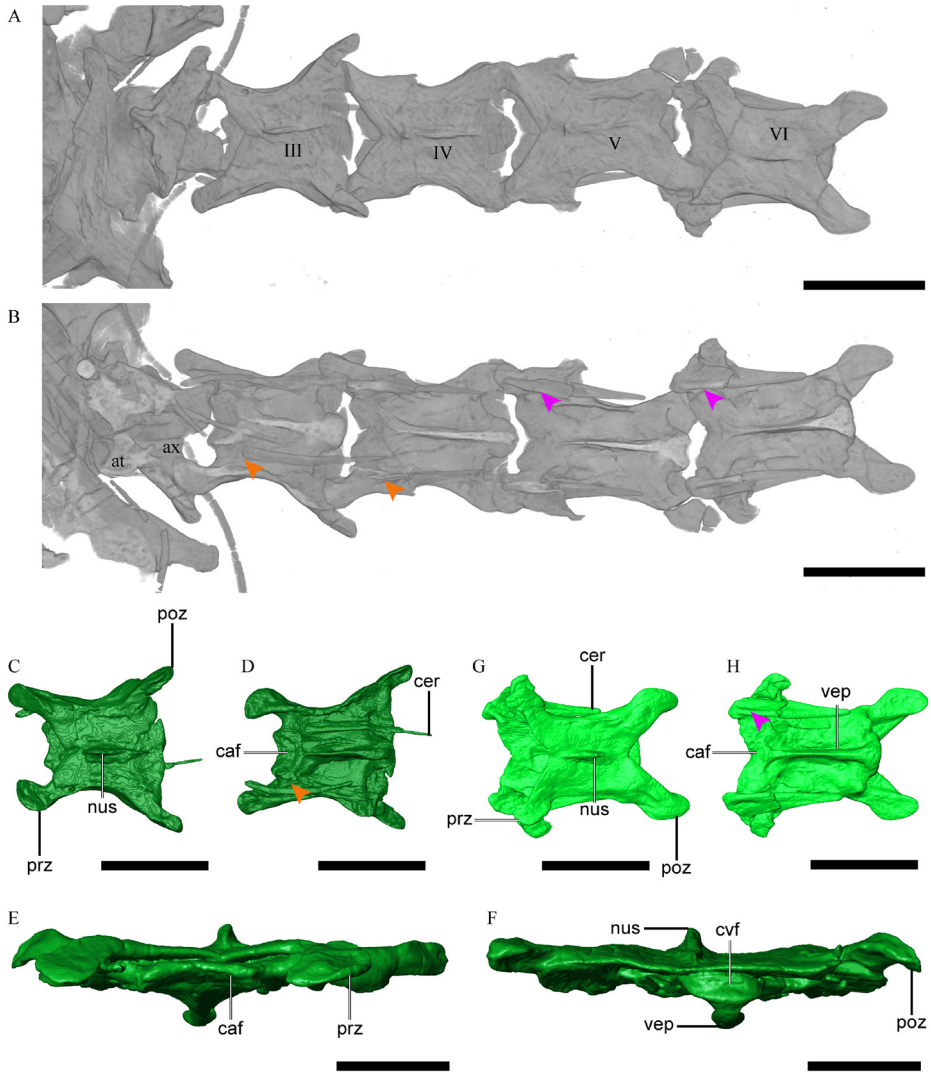

Fig. 8 Anatomy of cranial cervical vertebrae of *Parabohaiornis martini*, IVPP V28398
CT image of the cranialmost six cervicals in dorsal (A) and ventral (B) views, respectively. Digital reconstruction of the third cervical in dorsal (C), ventral (D), cranial (E) and caudal (F) views; the sixth cervical in dorsal (G) and ventral (H) views. The orange arrowheads in B and D denote the unfused cervical ribs and centra, and the purple arrowheads in B and H denote the fusion between the cervical ribs and centra
Abbreviations: at. atlas; ax. axis; caf. cranial articular facet of centrum; cer. cervical rib; cvf. caudal articular facet of centrum; nus. neural spine; poz. postzygapophysis; prz. prezygapophysis; vep. ventral process; III–VI. third to sixth cervicals. Scale bars = 5 mm (A–D, G, H); scale bars = 2 mm (G, H)

5 Discussion

The new specimen IVPP V28398 is referrable to the enantiornithine family Bohaiornithidae due to the following shared diagnostic features with the clade: the teeth are large and subconical with sharply tapered and slightly caudally recurved crowns; the omal

ends of the furcula are expanded; the scapular shaft is slightly bowed with a straight ventral margin and convex dorsal margin; the pygostyle gently tapers distally without an abrupt distal constriction; and the pedal digit II is much more robust than the other pedal digits (Figs. 1, 2) (Wang et al., 2014a). More specifically, V28398 can be referred to the bohaiornithid *Parabohaiornis martini* due to their overall comparable morphologies (including postcranial skeletons) and limb proportions (Table 1). In particularly, they preserve the following combination of characteristics that can distinguish this taxon from other bohaiornithids: the maxillary bears four teeth; the dorsal margin of the lacrimal is concave centrally; and the acromion process of the scapula extends cranially nearly parallel to the shaft in lateral view (Wang et al., 2014a).

The temporal and cranial base regions that are functionally vital to avian cranial kinesis are poorly investigated in early diverging avialans including many enantiornithines (Bock, 1964; Zusi, 1984; Holliday and Witmer, 2008; Gussekloo et al., 2017), with progress made in most recent studies (Hu et al., 2020; O'Connor et al., 2020; Wang et al., 2021, 2022; Li et al., 2023). On one hand, elements in these regions are delicate and thus are less likely to be preserved in great compared to other cranial elements (e.g., maxilla, dentary). On the other hand, most of the known early branching avialan fossils are only preserved in two-dimensions (e.g., Jehol specimens), severally limiting the data obtainable through traditional observation under microscopy. The well-preserved skull of the new specimen, visualized via high-resolution of x-ray CT, provides new data about the temporal and cranial base configurations in early avialans. The T-shaped postorbital with an elongate jugal process, and the dorsally directed caudal end of the jugal, likely constitute a complete postorbital bar that separates the orbital from the temporal fenestra. The free squamosal with a pronounced postorbital process articulates with the elongate squamosal process of the postorbital, forming a temporal bar that separates the supratemporal fenestra from the infratemporal fenestra. Therefore, an ancestrally diapsid temporal region is present in *Parabohaiornis*, as in *Longusunguis*, *Yuanchuavis*, and IVPP V12707 (Hu et al., 2020; Wang et al., 2021, 2022). However, the highly reduced squamosal process of the quadratojugal probably fails to reach the squamosal. This suggests that the infratemporal fenestra is confluent with the quadrate fenestra, which is guration (Currie, 1995; Holliday and Witmer, 2008). In contrast, the squamosal-quadratojugal contact is retained in the aforementioned enantiornithines (Hu et al., 2020; Wang et al., 2021, 2022). The loss of any squamosal-quadratojugal contact may have released some intracranial constraints, but the skull of *Parabohaiornis* is certainly akinetic given the presence of the postorbital and temporal bars, as well as the pronounced basipterygoid processes that severely restricted the sliding movements of the palatal elements (Holliday and Witmer, 2008; Gussekloo et al., 2017; Wang et al., 2022). Interestingly, the recent study of the *Yuanchuavis* cranial anatomy shows that its palatine is modified from the tetraradiate condition seen in *Archaeopteryx* and non-avialan theropods by the loss of the jugal process, which also helps to reduce the constraints imposed

on intracranial movements (Wang et al., 2022). These observations demonstrate independent experimentations that took place during the evolutionary assembly of kinetic skull in early avialan history. Future studies utilizing enhanced visualization approaches that encompass more specimens, most importantly the early diverging members of the Ornithuromorpha are needed to piece together the tempo and patterns of structural modifications that led to the modern avian skull.

Acknowledgments We thank YIN Pengfei, MIAO Song, and FENG Jiutong for helping in CT scanning. We Thank Jingmai K.O'Connor and LI Zhiheng for constructive comments that help to improve the manuscript. This research is supported by the National Natural Science Foundation of China (42225201), the Key Research Program of Frontier Sciences, CAS (ZDBS-LY-DQC002), and the Tencent Foundation (through the XPLORER PRIZE)

马氏副渤海鸟(鸟翼类：反鸟类)新标本对鸟类头骨早期演化的意义

王　敏[1,2]

(1中国科学院古脊椎动物与古人类研究所，中国科学院脊椎动物演化与人类起源重点实验室 北京 100044)

(2 中国科学院生物演化与环境卓越创新中心 北京 100044)

摘要：反鸟类是目前已知物种多样性最丰富的中生代鸟类类群，已有超过60个反鸟类物种在近乎所有的大洲相继被发现，其存续时间贯穿整个白垩纪。多数反鸟类以及其他早期鸟翼类的化石材料多以二维平面的形式保存，而且鸟翼类头骨的骨骼大都轻薄而不易保存为化石，这些因素对研究早期鸟类头骨的形态学特征造成很大困难。早期鸟翼类头骨化石的稀缺极大的限制了关于恐龙相对笨重和非可动性的头骨与鸟类质轻而具有可动性的头骨之间如何演化的研究。报道了一件新的反鸟类渤海鸟科马氏副渤海鸟(*Parabohaiornis martini*)的新标本，并对其头骨形态进行了三维复原。研究结果显示副渤海鸟保留了原始的非鸟类恐龙所具有的颞区和腭区结构，进一步证实了上述头骨区域在演化上相对保守，以及多数鸟翼类原始类群仍然保留了非可动性头骨这一最近提出的假说。

关键词：鸟翼类，渤海鸟科，头骨，头骨可动性，反鸟类

References

Barsbold R, 1974. Saurornithoididae, a new family of small theropod dinosaurs from central Asia and North America. Palaeontol Pol, 30: 5–22

Barsbold R, Osmólska H, 1999. The skull of *Velociraptor* (Theropoda) from the Late Cretaceous of Mongolia. Acta Palaeontol Pol, 44: 189–219

Baumel J J, Witmer L M, 1993. Osteologia. In: Baumel J J, King A S, Breazile J E et al. eds. Handbook of Avian Anatomy: Nomina Anatomica Avium, 2nd ed. Cambridge, U.K.: Nuttall Ornithological Club. 45–132

Bertelli S, Giannini N P, Ksepka D T, 2006. Redescription and phylogenetic position of the Early Miocene penguin *Paraptenodytes antarcticus* from Patagonia. Am Mus Novit, 36: 1–36

Bock W J, 1964. Kinetics of the avian skull. J Morphol, 114: 1–41

Chiappe L M, Ji S A, Ji Q, 2007. Juvenile birds from the Early Cretaceous of China: implications for enantiornithine ontogeny. Am Mus Novit, 3594: 1–46

Chiappe L M, Meng Q J, Serrano F et al., 2019. New *Bohaiornis*-like bird from the Early Cretaceous of China:

Currie P J, 1995. New information on the anatomy and relationships of *Dromaeosaurus albertensis* (Dinosauria: Theropoda). J Vert Paleont, 15: 576–591

Currie P J, Zhao X J, 1993. A new carnosaur (Dinosauria, Theropoda) from the Jurassic of Xinjiang, People's Republic of China. Can J Earth Sci, 30: 2037–2081

Elżanowski A, 1991. New observations of the skull of *Hesperornis* with reconstructions of the bony palate and otic region. Postilla, 207: 1–20

Elżanowski A, Stidham T A, 2011. A galloanserine quadrate from the Late Cretaceous Lance Formation of Wyoming. Auk, 128: 138–145

Elżanowski A, Wellnhofer P, 1996. Cranial morphology of *Archaeopteryx*: evidence from the seventh skeleton. J Vert Paleont, 16: 81–94

Gingerich P

Gussekloo S W S, Berthaume M A, Pulaski D R et al., 2017. Functional and evolutionary consequences of cranial fenestration in birds. Evolution, 71: 1327–1338

Hendrickx C, Araújo R, Mateus O, 2015. The non-avian theropod quadrate I: standardized terminology with an overview of the anatomy and function. PeerJ, 3: e1245

Holliday C M, Witmer L M, 2008. Cranial kinesis in dinosaurs: intracranial joints, protractor muscles, and their for cranial evolution and function in diapsids. J Vert Paleont, 28: 1073–1088

Hu D Y, Li L, Hou L H et al., 2011. A new enantiornithine bird from the Lower Cretaceous of western Liaoning, China. J Vert Paleont, 31: 154–161

Hu H, O'Connor J K, Wang M et al., 2020. New anatomical information on the bohaiornithid *Longusunguis* and the presence of a plesiomorphic diapsid skull in Enantiornithes. J Syst Palaeontol, 18: 1481–1495

Li Z H, Wang M, Stidham T A et al., 2023. Decoupling the skull and skeleton in a Cretaceous bird with unique appendicular morphologies. Nat Ecol Evol, 7: 20–31

Livezey B C, Zusi R L, 2006. Higher-order phylogeny of modern birds (Theropoda, Aves: Neornithes) based on comparative anatomy: I. methods and characters. Bull Carnegie Mus Nat Hist, 37: 1–544

Livezey B C, Zusi R L, 2007. Higher-order phylogeny of modern birds (Theropoda, Aves: Neornithes) based on comparative anatomy. II. Analysis and discussion. Zool J Linn Soc, 149: 1–95

Lovette I J, Fitzpatrick J W, 2016. Handbook of Bird Biology, 3rd ed. Chichester: John Wiley & Sons. 1–716

Lucas F A, 1903. Notes on the osteology and relationship of the fossil birds of the genera *Hesperornis*, *Hargeria*, *Baptornis*, and *Diatryma*. Proc U S Nat Mus, 26: 545–556

McDowell S, 1948. The bony palate of birds. Part I. The Palaeognathae. Auk: 520–549

Norell M A, Clark J M, Turner A H et al., 2006. A new dromaeosaurid theropod from Ukhaa Tolgod (Ömnögov, Mongolia). Am Mus Novit, 3545: 1–51

O'Connor J K, Chiappe L M, 2011. A revision of enantiornithine (Aves: Ornithothoraces) skull morphology. J Syst Palaeontol, 9: 135–157

O'Connor J K, Zhang Y G, Chiappe L M et al., 2013. A new enantiornithine from the Yixian Formation with the first recognized avian enamel specialization. J Vert Paleont, 33: 1–12

O'Connor P M, Turner A H, Groenke J R et al., 2020. Late Cretaceous bird from Madagascar reveals unique development of beaks. Nature, 588: 272–276

Ostrom J H, 1969. Osteology of *Deinonychus antirrhopus*, an unusual theropod from the Lower Cretaceous of Montana. Bull Peabody Mus Nat Hist, 30: 1–165

Rauhut O W M, 2003. The interrelationships and evolution of basal theropods. Spec Pap Palaeontol, 69: 1–213

Rauhut O W M, 2014. New observations on the skull of *Archaeopteryx*. Paläontol Z, 88: 211–221

Stidham T A, O'Connor J K, 2021. The evolutionary and functional implications of the unusual quadrate of *Longipteryx chaoyangensis* (Avialae: Enantiornithes) from the Cretaceous Jehol Biota of China. J Anat, 239: 1066–1074

Sullivan C, Xu X, 2017. Morphological diversity and evolution of the jugal in dinosaurs. Anat Rec., 300: 30–48

Wang M, Hu H, 2017. A comparative morphological study of the jugal and quadratojugal in early birds and their dinosaurian relatives. Anat Rec, 300: 62–75

Wang M, Zhou Z H, O'Connor J K et al., 2014a. A new diverse enantiornithine family (Bohaiornithidae fam. nov.) from the Lower Cretaceous of China with information from two new species. Vert PalAsiat, 52: 31–76

Wang M, O'Connor J K, Zhou Z H, 2014b. A new robust enantiornithine bird from the Lower Cretaceous of China with scansorial adaptations. J Vert Paleont, 34: 657–671

Wang M, Stidham T A, Li Z H et al., 2021. Cretaceous bird with dinosaur skull sheds light on avian cranial evolution. Nat Commun, 12: 3890

Wang M, Stidham T A, O'Connor J K et al., 2022. Insight into the evolutionary assemblage of cranial kinesis from a Cretaceous bird. eLife, 11: e81337

Wang X R, O'Connor J K, Zhao B et al., 2010. New species of Enantiornithes (Aves: Ornithothoraces) from the Qiaotou Formation in Northern Hebei, China. Acta Geol Sin, 84: 247–256

Weishampel B D, Dodson P, Osmólska H, 2004. The Dinosauria, 2nd ed. Berkeley: University of California Press. 1–880

Witmer L, 1997. Craniofacial air sinus systems. In: Currie P J, Padian K eds. Encyclopedia Dinosauria. New York: Academic Press. 151–159

Yu Z Q, Wang M, Li Y et al., 2021. New geochronological constraints for the Lower Cretaceous Jiufotang Formation in Jianchang basin, NE China, and their implications for the late Jehol Biota. Palaeogeogr Palaeoclimatol Palaeoecol, 583: 110657

Zhang Z H, Chiappe L M, Han G et al., 2013. A large bird from the Early Cretaceous of China: new information on the skull of enantiornithines. J Vert Paleont, 33: 1176–1189

Zhou Z H, Clarke J, Zhang F C, 2008. Insight into diversity, body size and morphological evolution from the largest Early Cretaceous enantiornithine bird. J Anat, 212: 565–577

Zhou Z H, Luis M C, Zhang F C, 2005. Anatomy of the Early Cretaceous bird *Eoenantiornis buhleri* (Aves : Enantiornithes) from China. Can J Earth Sci, 42: 1331–1338

Zusi R L, 1984. A functional and evolutionary analysis of rhynchokinesis in birds. Smithson Contrib Zool, 395: 1–40